Table S1. Experimental parameters and refinement details for the structures of **Nd**, **Ho**, **Tm** at 100 and 300K.

Identification code	**Nd_100K**	**Nd_300K**	**Ho_100K**
Deposition number (CCDC)	2528619	2528623	2528620
Empirical formula	$C_{27}H_{29}N_2NdO_6$	$C_{27}H_{29}N_2NdO_6$	$C_{27}H_{29}HoN_2O_6$
Formula weight	621.76	621.76	642.45
Temperature/K	100(2)	300(2)	100(2)
Crystal system	monoclinic	monoclinic	monoclinic
Space group	$P2_1/n$	$P2_1/n$	$P2_1/n$
a/Å	9.4200(9)	9.520(5)	9.4176(7)
b/Å	20.973(2)	21.161(11)	20.7896(10)
c/Å	14.6628(14)	14.926(7)	14.4163(11)
α/°	90	90	90
β/°	98.810(3)	99.216(16)	98.198(3)
γ/°	90	90	90
Volume/Å^3	2862.8(5)	2968(3)	2793.7(3)
Z	4	4	4
ρ_{calc}g/cm^3	1.443	1.391	1.527
μ/mm^{-1}	1.853	1.787	2.873
F(000)	1252.0	1252.0	1280.0
Crystal size/mm^3	0.24 × 0.08 × 0.03	0.24 × 0.08 × 0.03	0.24 × 0.08 × 0.03
Radiation	MoKα (λ = 0.71073)	MoKα (λ = 0.71073)	MoKα (λ = 0.71073)
2Θ range for data collection/°	3.884 to 50.496	4.74 to 50.498	3.918 to 53.998
Index ranges	-11 ≤ h ≤ 11 0 ≤ k ≤ 25 0 ≤ l ≤ 17	-11 ≤ h ≤ 11 -25 ≤ k ≤ 25 -17 ≤ l ≤ 17	-12 ≤ h ≤ 12 -26 ≤ k ≤ 22 -18 ≤ l ≤ 18
Reflections collected	5190	48426	25790
Independent reflections	5190 [R_{int} = 0.0980, R_{sigma} = 0.0805]	5371 [R_{int} = 0.1147 R_{sigma} = 0.0568]	6086 [R_{int} = 0.0465, R_{sigma} = 0.0426]
Data/restraints/parameters	5190/0/332	5371/7/331	6086/0/331
Goodness-of-fit on F^2	1.083	1.071	1.067
Final R indexes [I>=2σ (I)]	R_1 = 0.0467 wR_2 = 0.0822	R_1 = 0.0401 wR_2 = 0.0763	R_1 = 0.0378 wR_2 = 0.0738
Final R indexes [all data]	R_1 = 0.0797 wR_2 = 0.0986	R_1 = 0.0794 wR_2 = 0.0970	R_1 = 0.0464 wR_2 = 0.0767
Largest diff. peak/hole / e Å^{-3}	1.20/-0.73	0.98/-0.59	1.38/-1.28

Table S1 (continued).

Identification code	**Ho_300K**	**Tm_100K**	**Tm_300K**
Deposition number (CCDC)	2528622	2528621	2528624
Empirical formula	$C_{27}H_{29}HoN_2O_6$	$C_{27}H_{29}N_2O_6Tm$	$C_{27}H_{29}N_2O_6Tm$
Formula weight	642.45	646.45	646.45
Temperature/K	300(2)	100(2)	300(2)
Crystal system	monoclinic	monoclinic	monoclinic
Space group	$P2_1/n$	$P2_1/n$	$P2_1/n$
a/Å	9.4837(7)	9.3976(4)	9.482(3)
b/Å	21.0014(14)	20.7896(9)	21.013(6)
c/Å	14.6551(10)	14.3501(6)	14.641(6)
α/°	90	90	90
β/°	98.797(2)	98.241(2)	98.921(18)
γ/°	90	90	90
Volume/Å^3	2884.5(3)	2774.7(2)	2881.8(17)
Z	4	4	4
ρ_{calc}g/cm^3	1.479	1.548	1.490
μ/mm^{-1}	2.782	3.238	3.118
F(000)	1280.0	1288.0	1288.0
Crystal size/mm^3	0.12 × 0.1 × 0.02	0.28 × 0.08 × 0.04	0.28 × 0.08 × 0.04
Radiation	MoKα (λ = 0.71073)	MoKα (λ = 0.71073)	MoKα (λ = 0.71073)
2Θ range for data collection/°	3.878 to 52.76	4.798 to 50.7	4.76 to 55.752
Index ranges	-11 ≤ h ≤ 11 -26 ≤ k ≤ 26 -18 ≤ l ≤ 18	-11 ≤ h ≤ 11 -25 ≤ k ≤ 25 -17 ≤ l ≤ 17	-12 ≤ h ≤ 12 -27 ≤ k ≤ 27 -19 ≤ l ≤ 19
Reflections collected	36092	41183	54804
Independent reflections	5894 [R_{int} = 0.0595 R_{sigma} = 0.0426]	5089 [R_{int} = 0.0768 R_{sigma} = 0.0427]	6883 [R_{int} = 0.0570 R_{sigma} = 0.0340]
Data/restraints/parameters	5894/7/331	5089/0/331	6883/6/331
Goodness-of-fit on F^2	1.197	1.033	1.048
Final R indexes [I>=2σ (I)]	R_1 = 0.0437 wR_2 = 0.0797	R_1 = 0.0314 wR_2 = 0.0624	R_1 = 0.0329 wR_2 = 0.0590
Final R indexes [all data]	R_1 = 0.0655 wR_2 = 0.0854	R_1 = 0.0420 wR_2 = 0.0657	R_1 = 0.0478 wR_2 = 0.0641
Largest diff. peak/hole / e Å^{-3}	0.70/-0.70	1.04/-1.13	1.07/-1.02

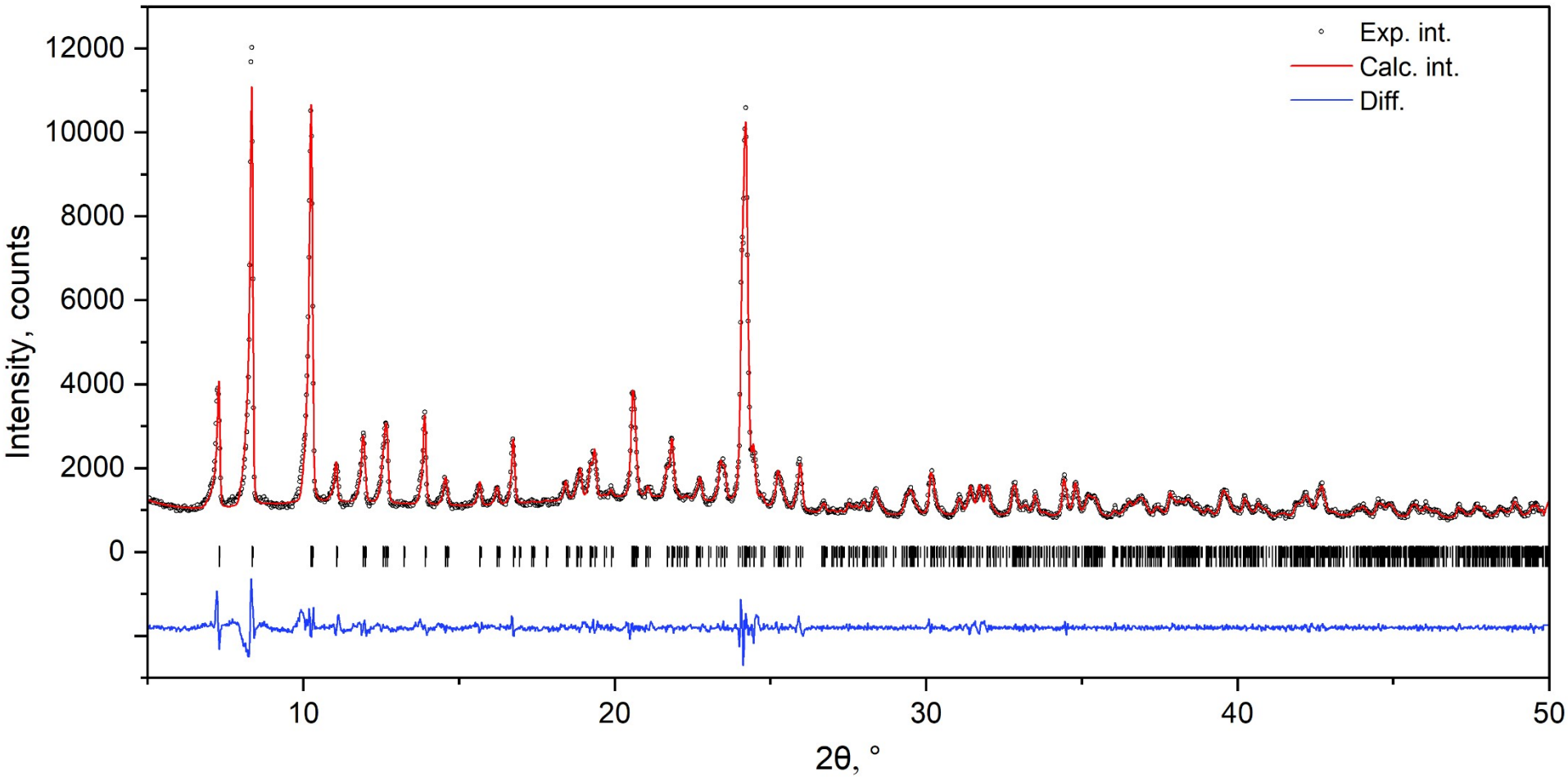

Fig. S1. Le Bail refinement results for powder pattern of **Nd**. The picture shows experimental (black round marks) and calculated (red line) data with difference curve (*I(exp)-I(calc)*, blue line) and CuK_{a1} (major black ticks) and CuK_{a2} (minor black ticks) peaks positions.

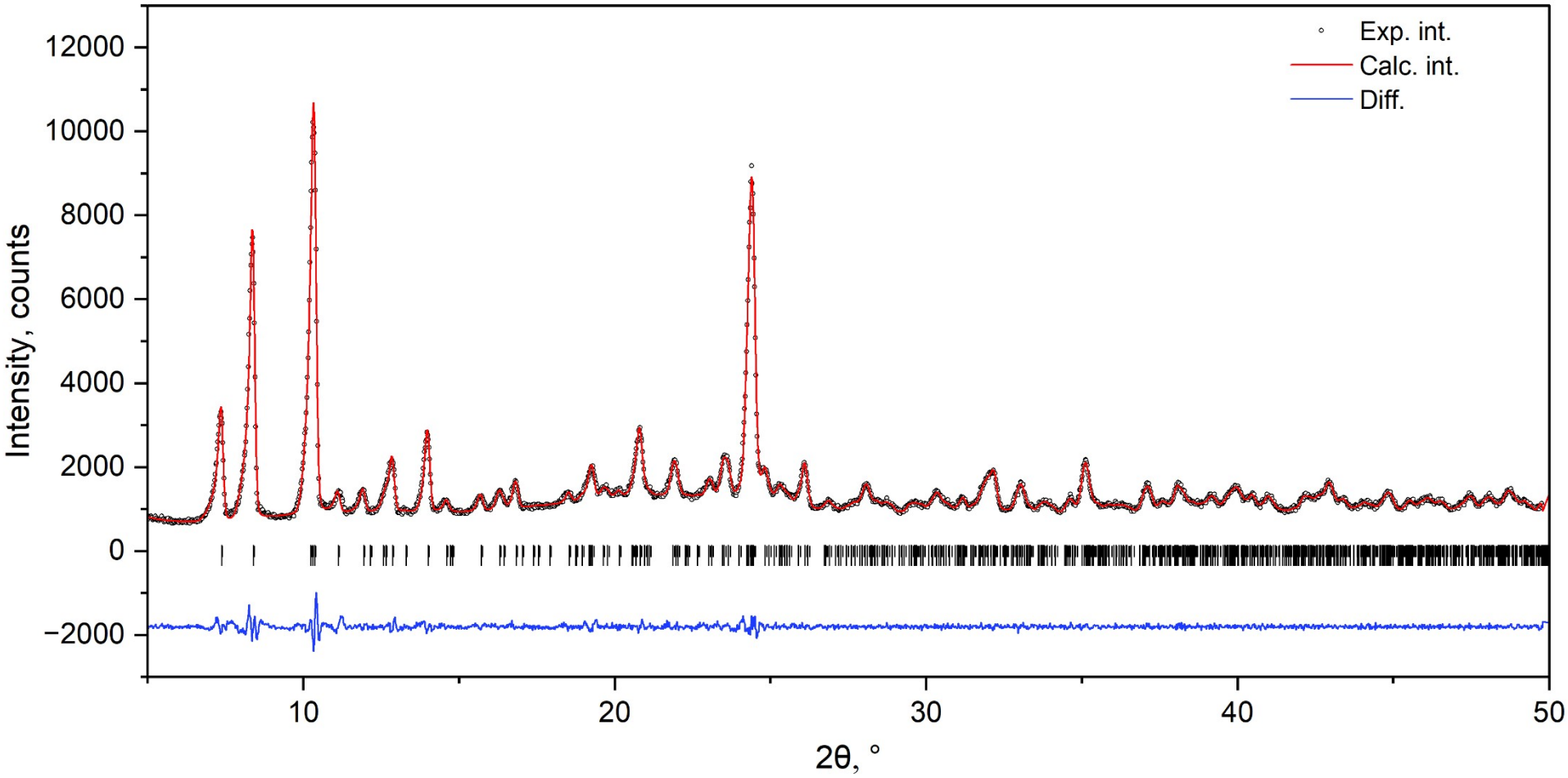

Fig. S2. Le Bail refinement results for powder pattern of **Ho**. The picture shows experimental (black round marks) and calculated (red line) data with difference curve (*I(exp)-I(calc)*, blue line) and CuK_{a1} (major black ticks) and CuK_{a2} (minor black ticks) peaks positions.

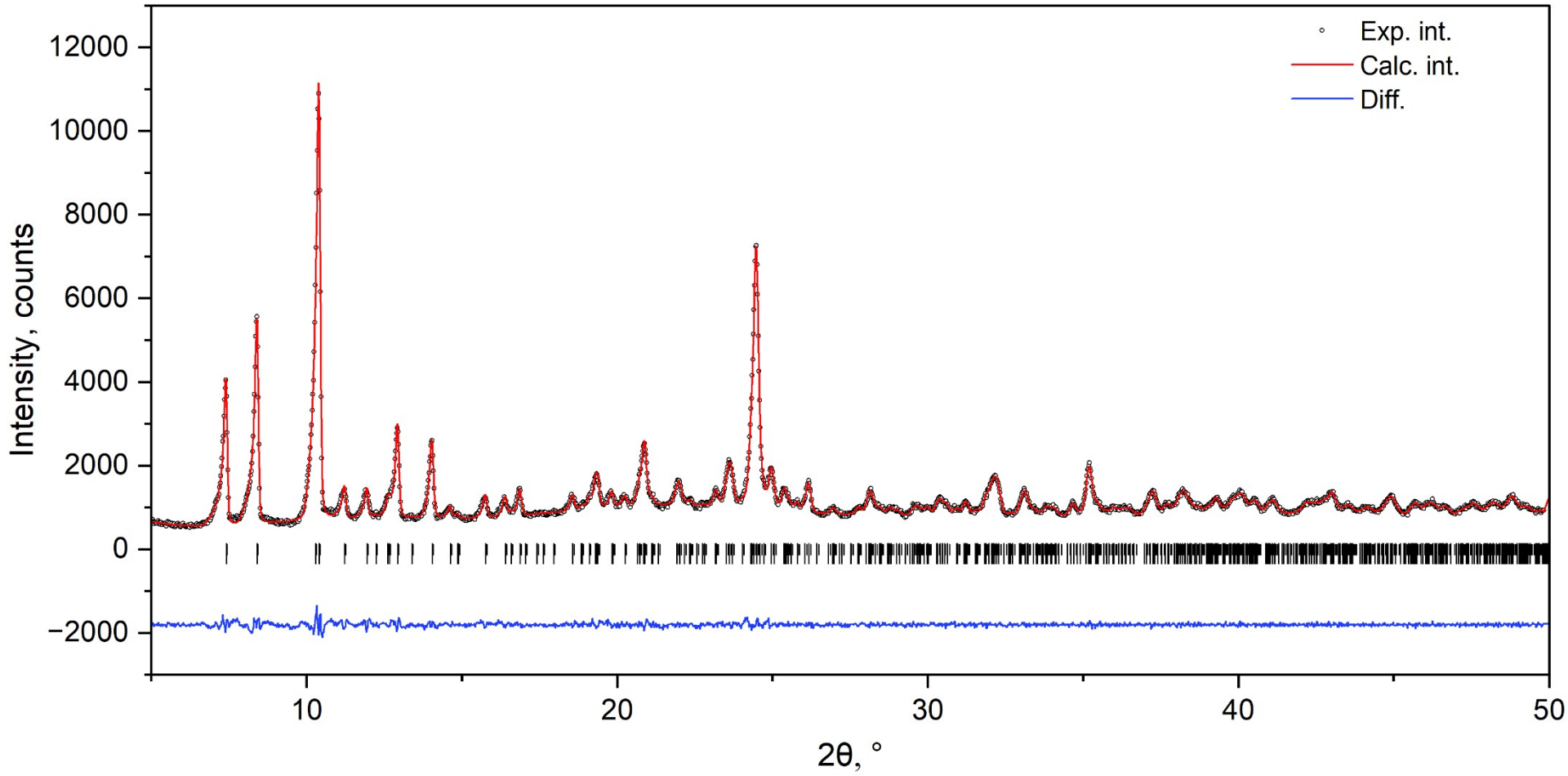

Fig. S3. Le Bail refinement results for powder pattern of **Tm**. The picture shows experimental (black round marks) and calculated (red line) data with difference curve (*I(exp)-I(calc)*, blue line) and CuK_{a1} (major black ticks) and CuK_{a2} (minor black ticks) peaks positions.

Table S2. Le Bail refinement indicators and refined parameters for powder patterns of polycrystalline samples of complexes synthesized.

Sample	SG	*a*, Å	*b*, Å	*c*, Å	*α*, °	*β*, °	*γ*, °	R_p	wR_p	GOF
Nd	$P2_1/n$	9.5783(6)	21.1574(7)	14.9666(6)	90	99.488(6)	90	3.55	5.07	1.87
Ho	$P2_1/n$	9.5917(7)	21.0569(14)	14.7422(9)	90	99.190(7)	90	2.84	3.80	1.41
Tm	$P2_1/n$	9.5285(7)	21.0098(11)	14.6330(9)	90	98,605(6)	90	2.84	3.79	1.29

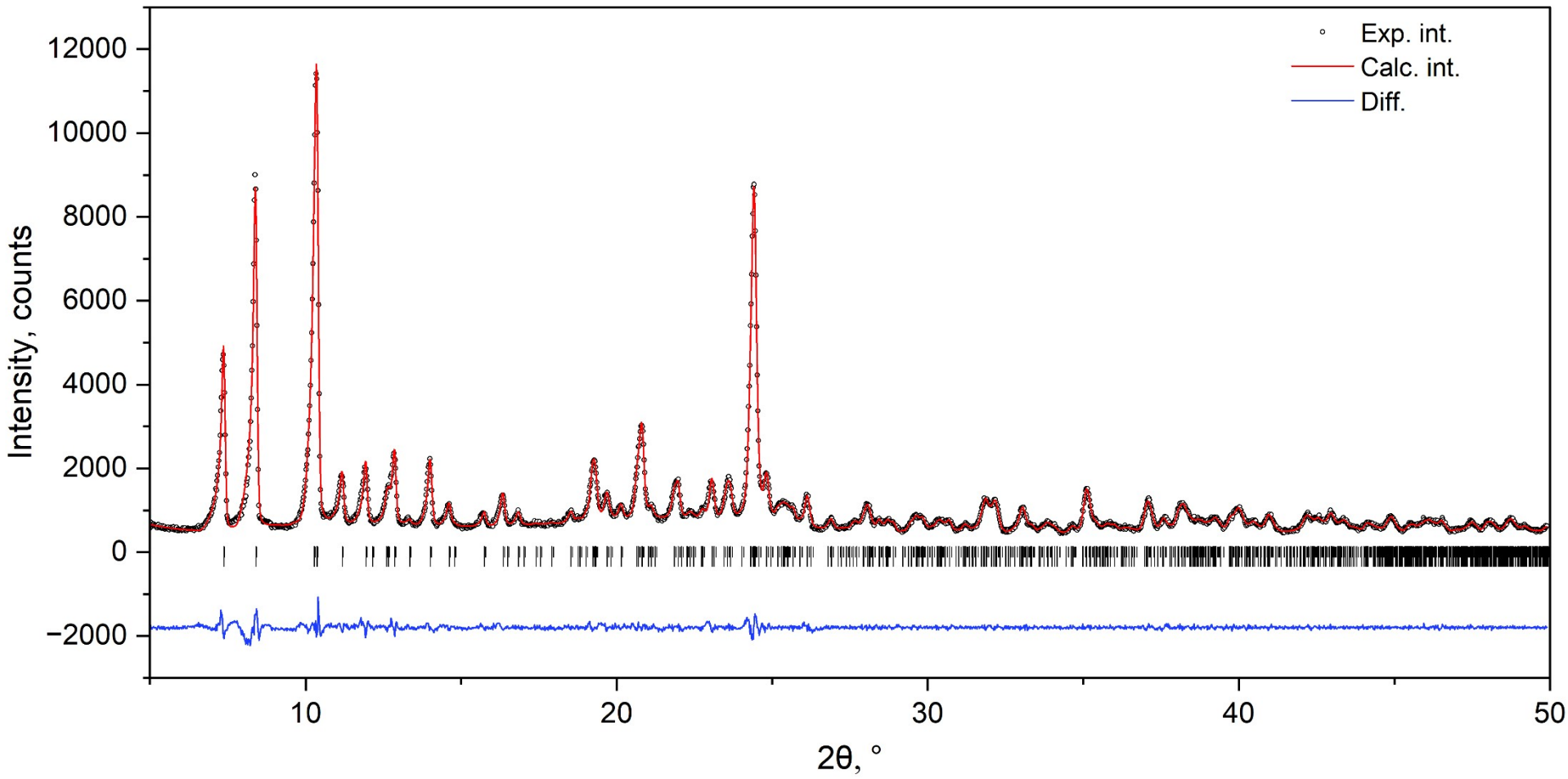

Fig. S4. Le Bail refinement results for powder pattern of **Nd@Y**. The picture shows experimental (black round marks) and calculated (red line) data with difference curve (*I(exp)-I(calc)*, blue line) and CuK_{a1} (major black ticks) and CuK_{a2} (minor black ticks) peaks positions.

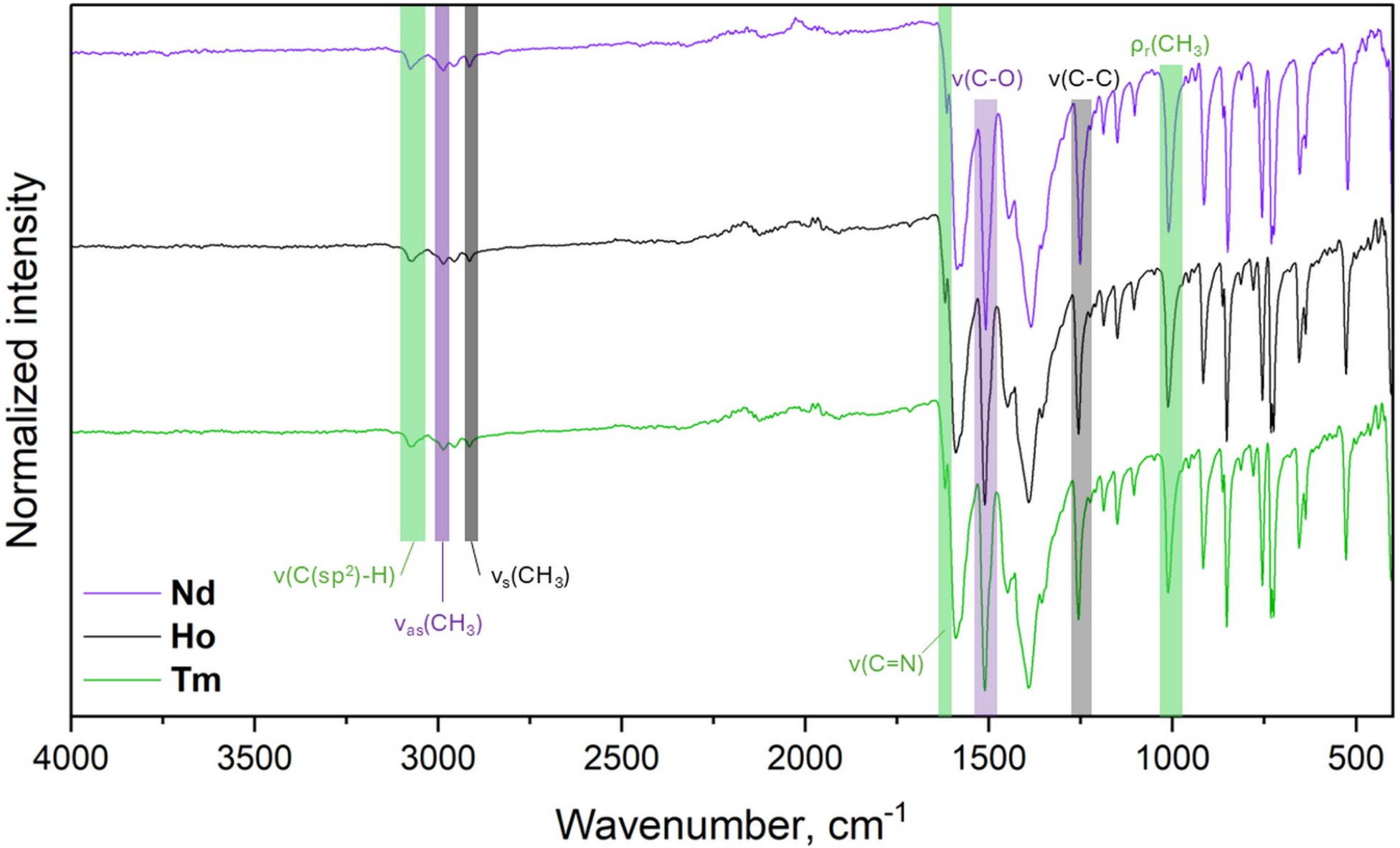

Fig. S5.Normalized ATR-IR spectra of **Nd**, **Ho** and **Tm** with the assignments for the most characteristic bands.

Table S3.SHAPE calculations for structures studied at 100 and 300K.

Structure	OP-8	HPY-8	HBPY-8	CU-8	SAPR-8	TDD-8	JGBF-8	JETBPY-8	JBTPR-8	BTPR-8	JSD-8	TT-8	ETBPY-8
Nd_100K	30.932	22.172	17.063	10.197	**0.603**	2.697	16.875	28.243	2.920	2.455	5.446	11.038	23.451
Nd_300K	30.667	22.108	16.921	9.838	**0.576**	2.656	16.830	28.194	3.062	2.532	5.697	10.596	23.211
Ho_100K	29.668	22.581	16.559	9.792	**0.375**	2.238	17.013	28.107	2.704	2.226	4.951	10.646	24.032
Ho_300K	29.866	22.661	16.596	9.822	**0.391**	2.529	17.012	28.027	2.912	2.425	5.286	10.671	23.936
Tm_100K	29.411	22.795	16.539	9.840	**0.353**	2.187	16.835	27.924	2.688	2.229	4.836	10.673	24.206
Tm_300K	29.808	22.745	16.582	9.870	**0.396**	2.458	16.925	28.000	2.901	2.449	5.191	10.718	24.100

Reference shapes

Coordination number = 8

OP-8 (D_{8h}) – Octagon

HPY-8 (C_{7v}) – Heptagonal pyramid

HBPY-8 (D_{6h}) – Hexagonal bipyramid

CU-8 (O_h) – Cube

SAPR-8 (D4d) – Square antiprism

TDD-8 (D2d) – Triangular dodecahedron

JGBF-8 (D2d) – Johnson – Gyrobifastigium J26

JETBPY-8 (D3h) - Johnson – Elongated triangular bipyramid J14

JBTP-8 (C2v) - Johnson – Biaugmented trigonal prism J50

BTPR-8 (C2v) – Biaugmented trigonal prism

JSD-8 (D2d) – Snub Disphenoid J84

TT-8 (Td) – Triakis tetrahedron

ETBPY-8 (D3h) – Elongated trigonal bipyramid

Table S4. Geometric parameters of the square antiprismatic polyhedra in structures of **Nd**, **Ho** and **Tm** at 100 and 300 K.

Structure	**Nd_100K**	**Nd_300K**	**Ho_100K**	**Ho_300K**	**Tm_100K**	**Tm_300K**
Average rms deviation for $O_1O_2O_3O_4$, Å	0.041	0.025	0.033	0.015	0.039	0.024
Average rms deviation for $O_5O_6N_1N_2$, Å	0.000	0.005	0.018	0.006	0.016	0.002
Angle between antiprism bases, °	3.6	3.1	2.1	2.3	1.7	2.0
Range of the flatness angle, °	53.7-58.8	53.8-59.0	55.0-59.1	54.7-59.2	55.2-59.2	54.9-59.0
Average Ln-O distances, Å	2.403(4)	2.399(4)	2.312(3)	2.313(4)	2.291(3)	2.292(3)
Average Ln-N distances, Å	2.647(5)	2.650(5)	2.537(4)	2.549(5)	2.515(3)	2.538(3)

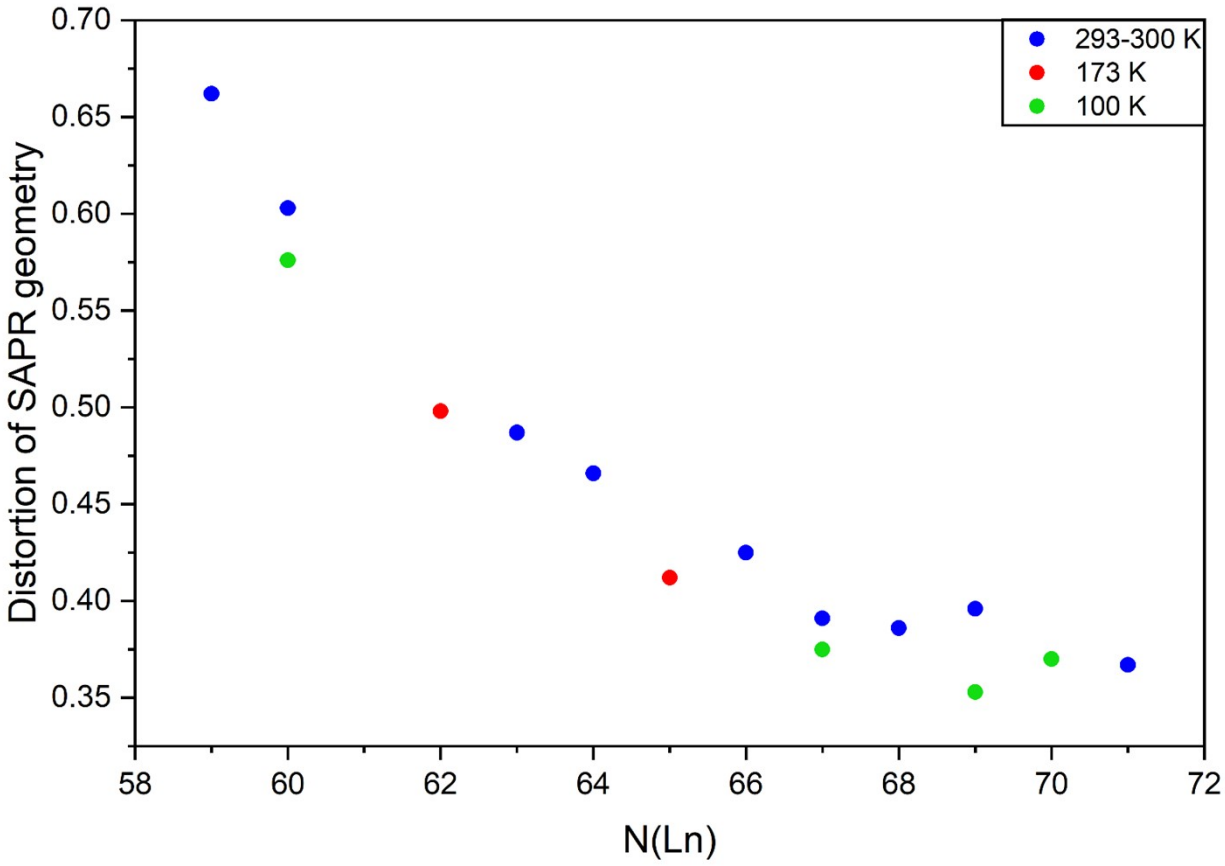

Fig. S6. The distortion of the coordination polyhedron in [Ln(acac)$_3$(phen)] structures as function of the lanthanide number.

Table S5. Selected bond lengths (Ln environment) for the studied structures.

Nd_100K			**Nd_300K**			**Ho_100K**		
Atom	**Atom**	**Length/Å**	**Atom**	**Atom**	**Length/Å**	**Atom**	**Atom**	**Length/Å**
Nd1	O6	2.368(4)	Nd1	O6	2.379(4)	Ho1	O6	2.288(3)
Nd1	O3	2.389(4)	Nd1	O3	2.388(4)	Ho1	O3	2.311(3)
Nd1	O4	2.419(4)	Nd1	O4	2.409(4)	Ho1	O4	2.321(3)
Nd1	O5	2.414(4)	Nd1	O5	2.401(4)	Ho1	O5	2.309(3)
Nd1	O2	2.399(4)	Nd1	O2	2.403(4)	Ho1	O2	2.311(3)
Nd1	N2	2.678(5)	Nd1	N2	2.667(5)	Ho1	N2	2.560(4)
Nd1	O1	2.429(4)	Nd1	O1	2.415(4)	Ho1	O1	2.334(3)
Nd1	N1	2.616(5)	Nd1	N1	2.633(4)	Ho1	N1	2.514(4)
Ho_300K			**Tm_100K**			**Tm_300K**		
Atom	**Atom**	**Length/Å**	**Atom**	**Atom**	**Length/Å**	**Atom**	**Atom**	**Length/Å**
Ho1	O6	2.292(4)	Tm1	O6	2.265(3)	Tm1	O6	2.269(3)
Ho1	O3	2.306(4)	Tm1	O3	2.284(3)	Tm1	O3	2.284(3)
Ho1	O4	2.328(4)	Tm1	O4	2.311(3)	Tm1	O4	2.311(3)
Ho1	O5	2.312(4)	Tm1	O5	2.290(3)	Tm1	O5	2.289(3)
Ho1	O2	2.304(4)	Tm1	O2	2.287(3)	Tm1	O2	2.288(3)
Ho1	N2	2.571(5)	Tm1	N2	2.539(3)	Tm1	N2	2.561(3)
Ho1	O1	2.335(4)	Tm1	O1	2.309(3)	Tm1	O1	2.309(3)
Ho1	N1	2.527(5)	Tm1	N1	2.490(3)	Tm1	N1	2.515(3)

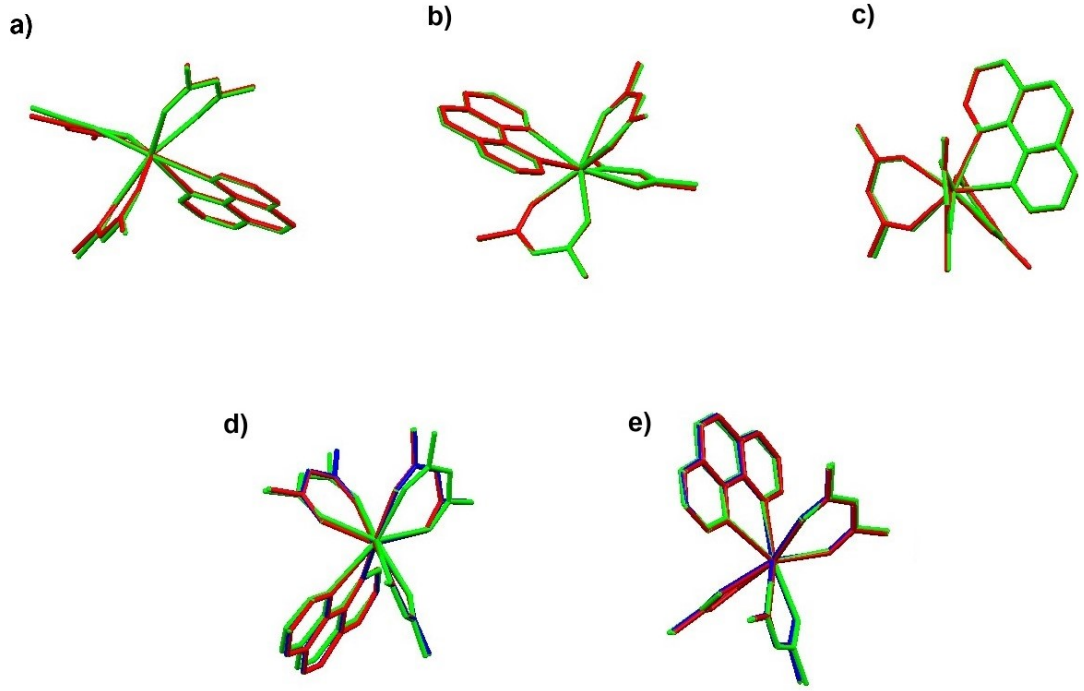

Fig. S7. Overlaying of the [Ln(acac)$_3$(phen)] fragments: a) **Nd_100K** (green) and **Nd_300K** (red); b) **Ho_100K** (green) and **Ho_300K**; c) **Tm_100K** (green) and **Tm_300K** (red); d) **Nd_100K** (green), **Ho_100K** (blue) and **Tm_100K** (red); e) **Nd_300K** (green), **Ho_300K** (blue) and **Tm_300K** (red).

Table S6. The shortest Ln…Ln distances in the studied structures.

Structure	Ln…Ln shortest distances		
Nd_100K	8.537(1)	9.064(1)	9.420(1)
Nd_300K	8.448(4)	9.122(5)	9.520(5)
Ho_100K	7.9708(8)	8.9852(8)	9.4176(8)
Ho_300K	8.2154(8)	9.0612(8)	9.4837(8)
Tm_100K	7.9460(6)	8.9614(6)	9.3976(5)
Tm_300K	8.188(3)	9.056(4)	9.482(4)

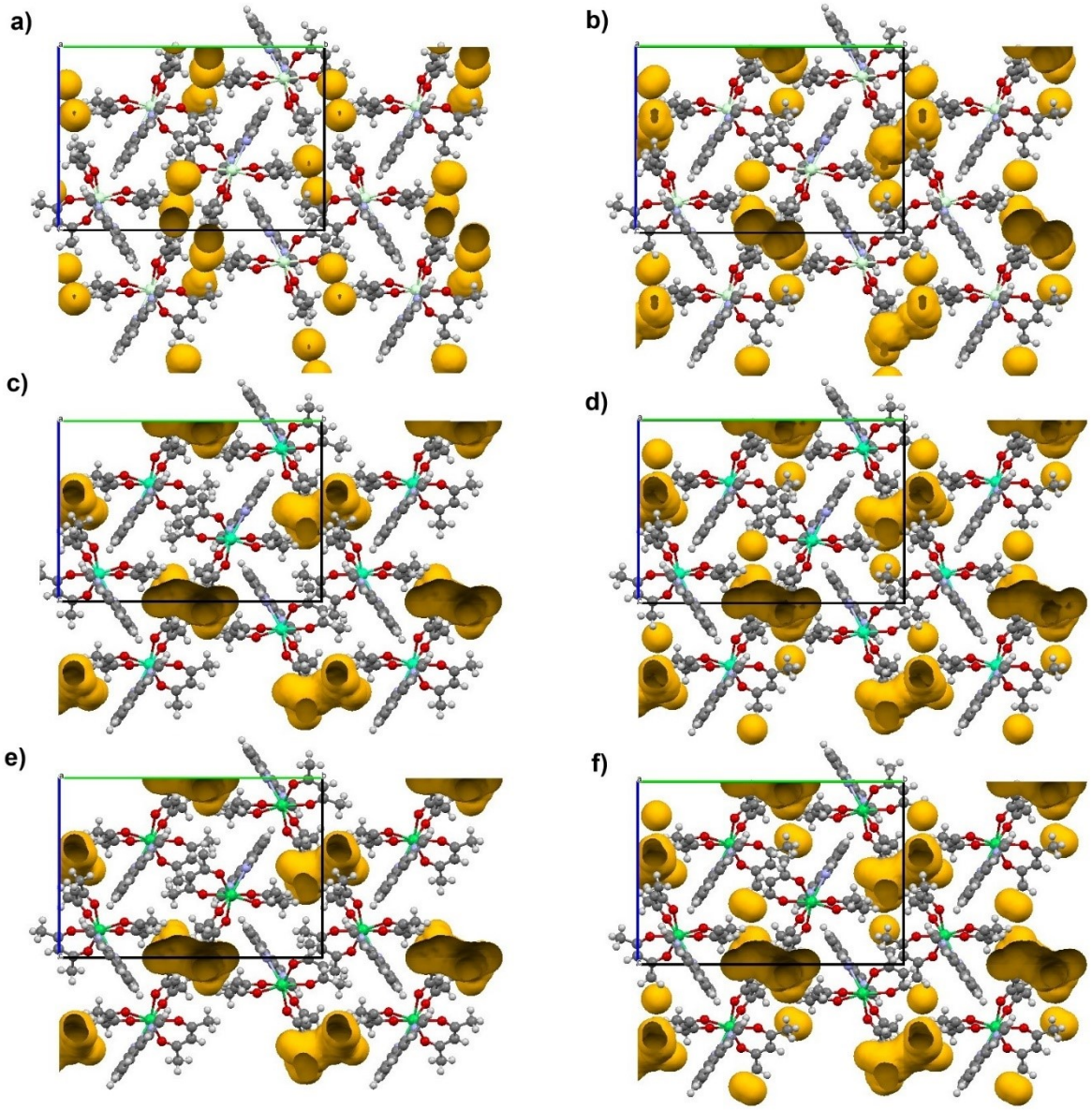

Fig. S8. Visualization of the voids (probe radius 1.2 Å) in structures **Nd_100K** (a), **Nd_300K** (b), **Ho_100K** (c), **Ho_300K** (d), **Tm_100K** (e) and **Tm_300K** (f).

Table S7. Voids (probe radius 1.2 Å) parameters in the structures of **Nd**, **Ho**, **Tm** at 100 and 300K.

Compound	Temperature, K	Unit cell volume, Å^3	Unit cell voids volume, Å^3	Voids fraction, %
Nd	100	2862.8(5)	100	3.5
Nd	300	2968(3)	155	5.2
Gd	293	2916.99(17)	198	6.8
Ho	100	2793.7(3)	197	7.0
Ho	300	2884.5(3)	215	7.5
Er	295	2881.0(6)	198	7.6
Tm	100	2774.7(2)	191	6.9
Tm	300	2881.8(17)	232	8.0

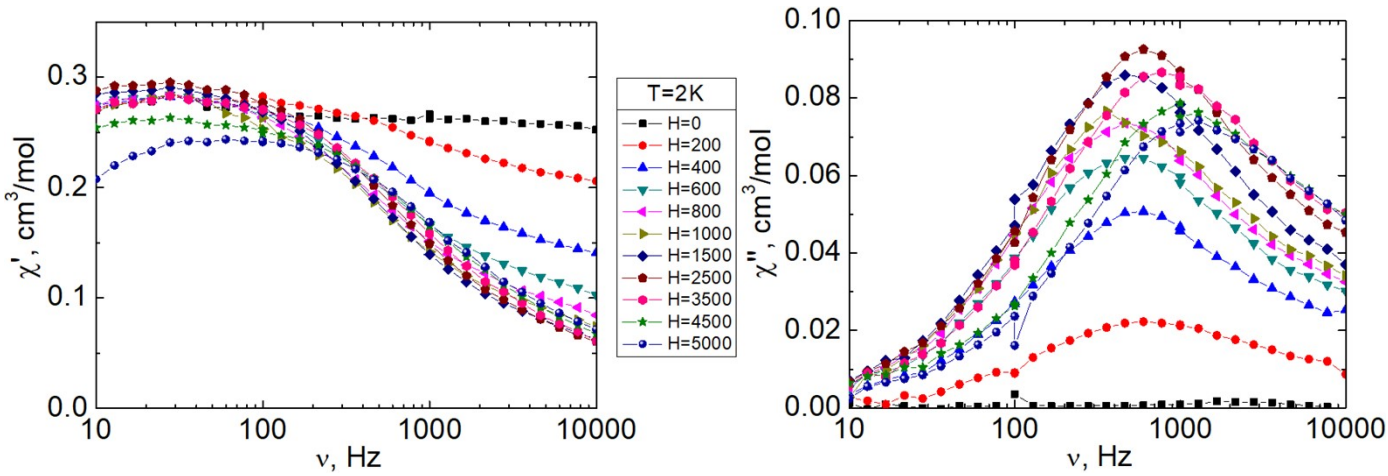

Fig. S9. Frequency dependencies of the in-phase (χ', left) and out-of-phase (χ'', right) components of the dynamic magnetic susceptibility of complex **Nd** measured at T=2K under various DC magnetic fields. Solid lines are visual guides.

Table S8. Various approximations of τ *vs.* 1/T dependency for complex **Nd** under a DC field of 1000 Oe.

Dependence of the relaxation time τ on the reciprocal temperature for Tb complex **1** (H = 1 kOe, T = 2–4 K).	Fit function, temperature range, and the best-fit parameters with uncertainties.
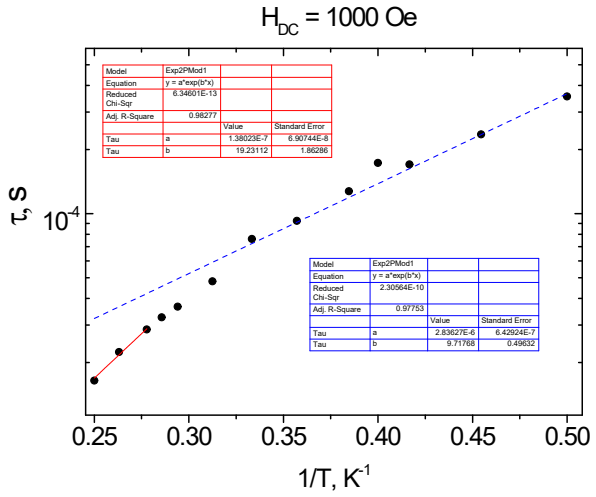	**Orbach** $\tau = \tau_0 \cdot \exp\{\Delta E/kT\}$ T = 3.6–4 K $\Delta E/k$ = 19±2 K $\tau_0 = 1.4 \cdot 10^{-7} \pm 7 \cdot 10^{-8}$ s R^2 = 0.98277(red line) **Meaningless fit!!!** T = 2-4 K $\Delta E/k$ = 9.7±0.5 K $\tau_0 = 2.8 \cdot 10^{-6} \pm 6 \cdot 10^{-7}$ s R^2 = 0.97753(blue line) **Meaningless fit!!!**
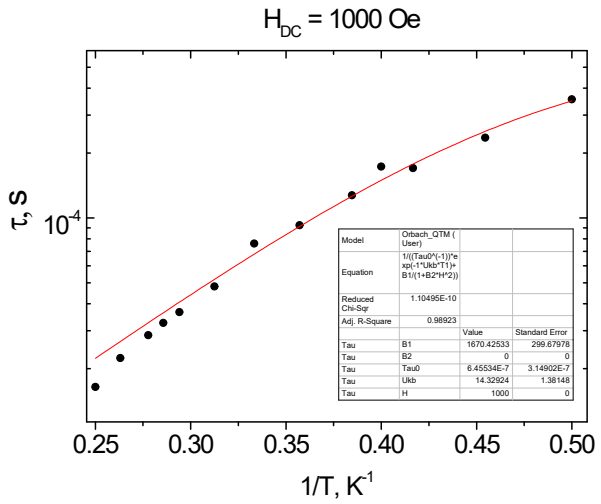	**Orbach+QTM** $\tau^{-1} = \tau_0^{-1} \cdot \exp\{-\Delta E/kT\}$+B T = 2-4 K $\Delta E/k$ = 14±1 K $\tau_0 = 6 \cdot 10^{-7} \pm 3 \cdot 10^{-7}$ s B= 1670± 300 s^{-1} R^2 = 0.98923 **Meaningless fit!!!**
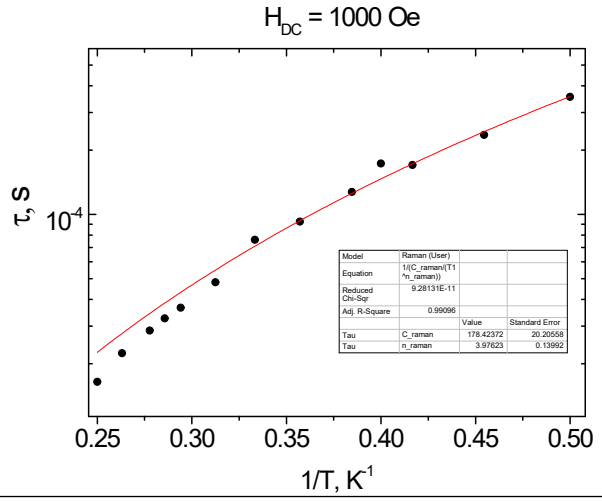	**Raman** $\tau^{-1} = C_{\mathrm{Raman}} T^{\mathrm{n\_Raman}}$ T = 2-4 K C_{Raman} = 178±20 $s^{-1}K^{-\mathrm{nRaman}}$ n_{Raman} = 4.0±0.1 R^2 = 0.99096

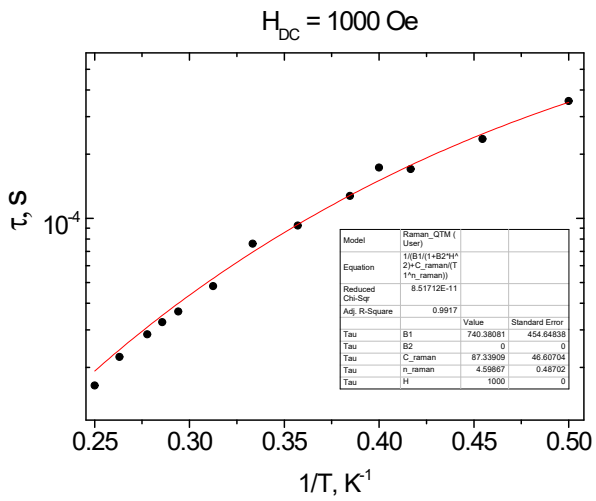

Raman+ QTM

$\tau^{-1} = C_{\text{Raman}} T^{\text{nRaman}} + \text{B}$

T = 2-4 K

C_{Raman} = 87±47 $s^{-1}K^{-\text{nRaman}}$

n_{Raman} = 4.6±0.5

B = 740±455 s^{-1}

R^2 = 0.9917

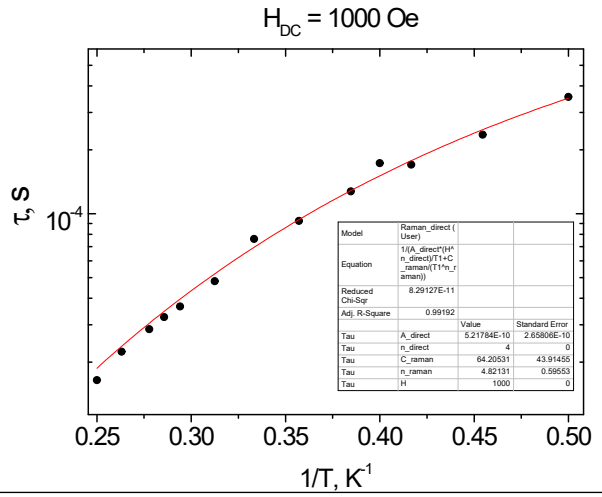

Raman+Direct

$\tau^{-1} = C_{\text{Raman}} T^{\text{nRaman}} + A_{direct} T H^4$

T = 2-4 K

C_{Raman} = 64±44 $s^{-1}K^{-\text{nRaman}}$

n_{Raman} = 4.8±0.6

A_{direct} = $5 \cdot 10^{-10} \pm 3 \cdot 10^{-10}$ $K^{-1}Oe^{-4}s^{-1}$

R^2 = 0.99192

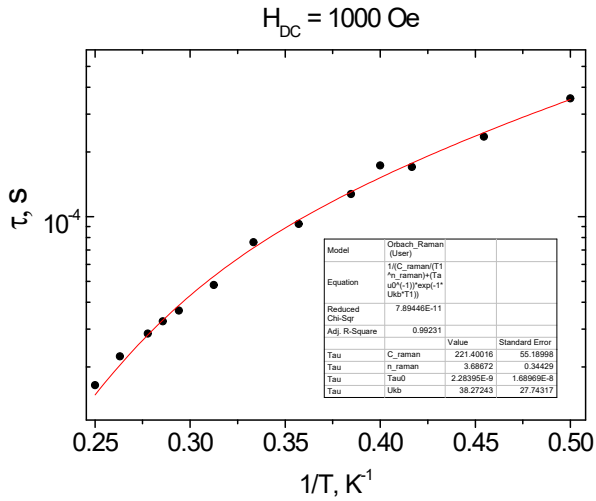

Orbach+Raman

$\tau^{-1} = \tau_0^{-1} \cdot \exp\{-\Delta E/kT\} + C_{\text{Raman}} T^{\text{nRaman}}$

T = 2-4 K

$\Delta E/k$ = 38±28 K

τ_0 = $2 \cdot 10^{-9} \pm 1.7 \cdot 10^{-8}$ s

C_{Raman} = 221±55 $s^{-1}K^{-\text{nRaman}}$

n_{Raman} = 3.7±0.3 (if n_{Raman} is not fixed, then it tends to be 0)

R^2 = 0.99231

Over-parametrization!!!

$\tau^{-1} = \tau_0^{-1} \cdot \exp\{-\Delta E/kT\} + C_{\text{Raman}} T^{\text{nRaman}}$

T = 2-4 K

$\Delta E/k$ = 31 K (fixed)

τ_0 = $1.6 \cdot 10^{-8} \pm 9 \cdot 10^{-9}$ s

C_{Raman} = 238±42 $s^{-1}K^{-\text{nRaman}}$

n_{Raman} = 3.6±0.2

R^2 = 0.99293

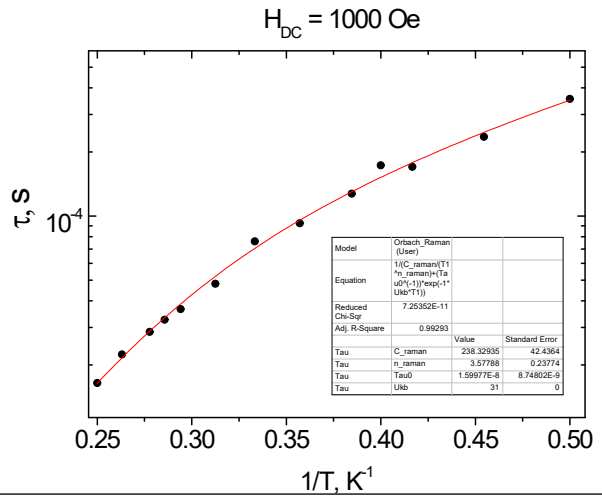

Meaningless fit!!!

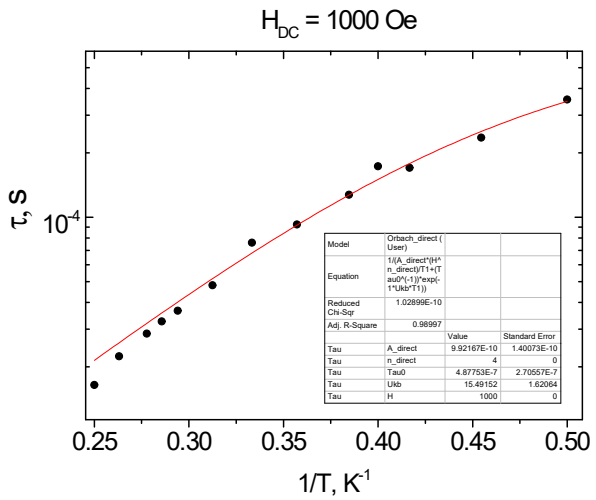

Orbach+Direct

$\tau^{-1} = \tau_0^{-1} \cdot \exp\{-\Delta E/kT\} + A_{direct} T H^4$

T = 2-4 K

$\Delta E/k$ = 15±2 K

$\tau_0 = 5 \cdot 10^{-7} \pm 3 \cdot 10^{-7}$ s

$A_{direct} = 1 \cdot 10^{-9} \pm 1 \cdot 10^{-10}$ $K^{-1}Oe^{-4}s^{-1}$

R^2 = 0.98997

Meaningless fit!!!

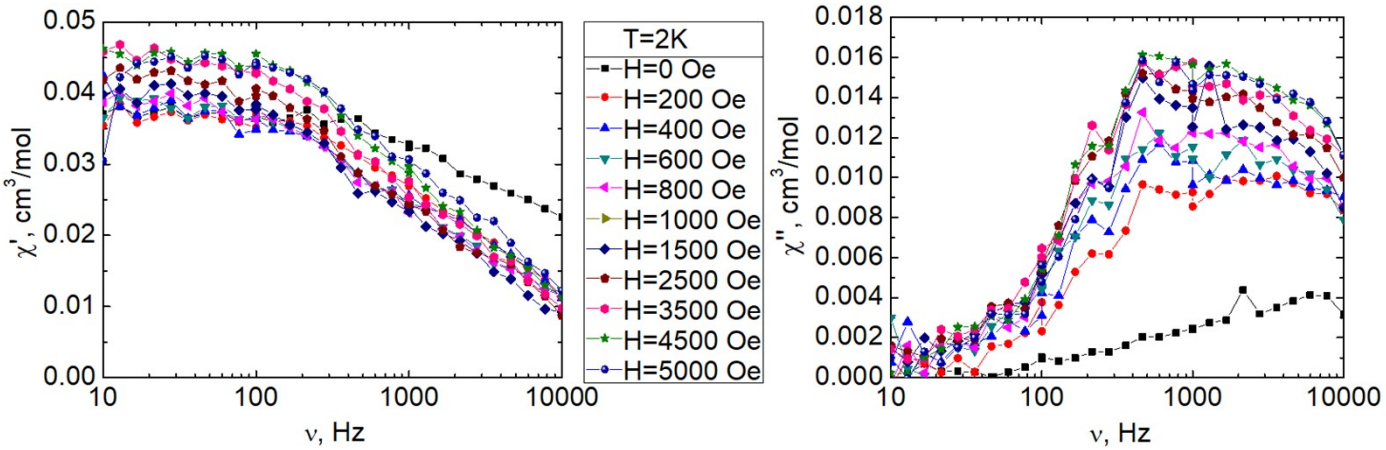

Fig. S10. Frequency dependencies of real (left) and imaginary (right) components of dynamic magnetic susceptibility of **Nd@Y** sample at 2 K in various DC magnetic fields. Solid lines are visual guides.

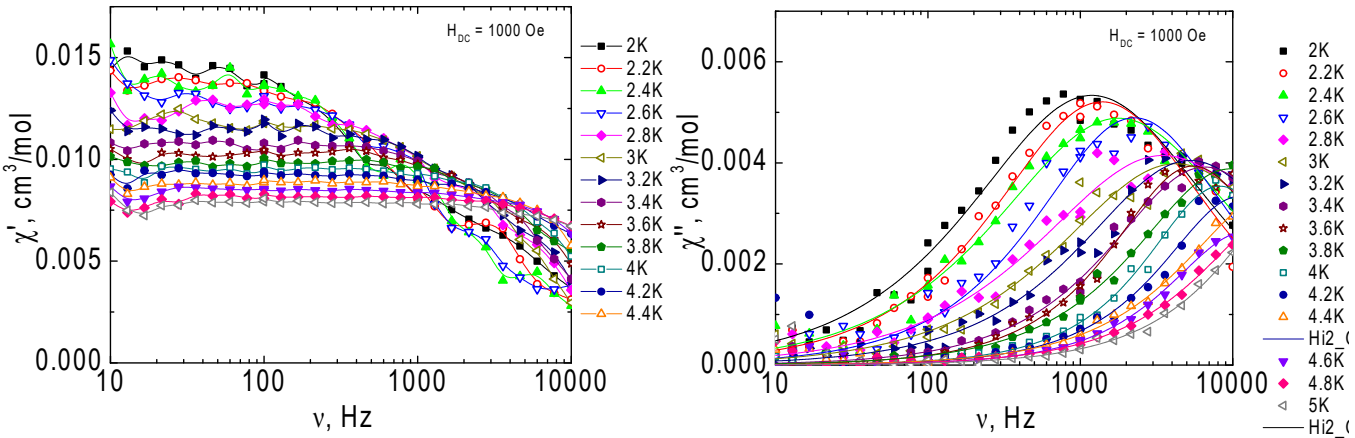

Fig. S11. Frequency dependencies of real (left) and imaginary (right) components of magnetic susceptibility for **Nd@Y** sample in 1000 Oe DC magnetic field. Solid lines on the left section are visual guides. Solid lines on the right section represent best fits by the generalized Debye model.

Table S9. Various approximations of τ *vs.* 1/T dependency for **Nd@Y** sample under a DC field of 1000 Oe.

Dependence of the relaxation time τ on the reciprocal temperature for Tb complex **1** (H = 1 kOe, T = 2–3.2 K).	Fit function, temperature range, and the best-fit parameters
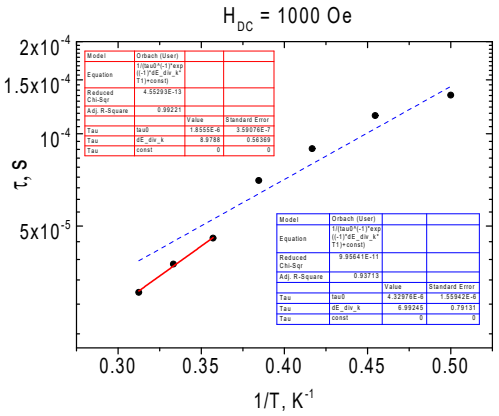	**Orbach** $\tau = \tau_0 \cdot \exp\{\Delta E/kT\}$ T = 2.8–3.2 K $\Delta E/k$ = 8.98 ± 0.56 K τ_0= 1.9·10^{-6} ± 4·10^{-7} s R^2 = 0.9922(red line) **Meaningless fit!!!** T = 2–3.2K $\Delta E/k$ = 7.0±0.8 K τ_0= 4.3·10^{-6} ±1.6·10^{-6} s R^2 = 0.93713(blue line) **Meaningless fit!!!**
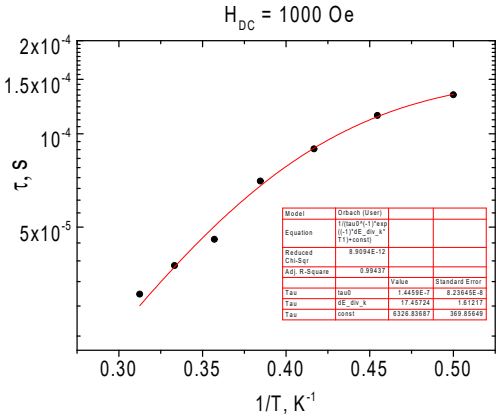	**Orbach+QTM** $\tau^{-1} = \tau_0^{-1} \cdot \exp\{-\Delta E/kT\}$+B T = 2–3.2K $\Delta E/k$ = 17±2 K τ_0= 1.4·10^{-7} ±8·10^{-8} s B= 6326± 369 s^{-1} R^2 = 0.9944 **Meaningless fit!!!**
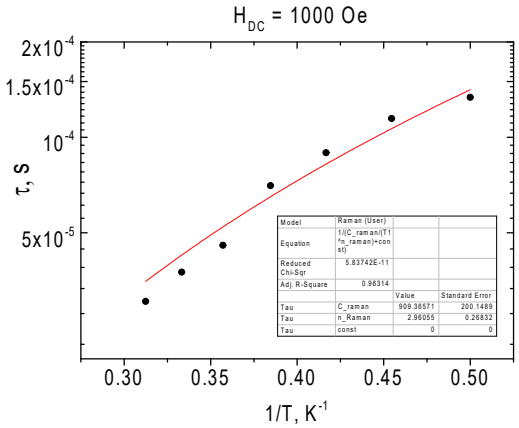	**Raman** $\tau^{-1} = C_{\text{Raman}} T^{\text{n\_Raman}}$ T = 2–3.2K C_{Raman}= 909±200 s^{-1}K$^{-\text{nRaman}}$ n$_{\text{Raman}}$= 2.96±0.26 R^2 = 0.96311 Moderate R^2

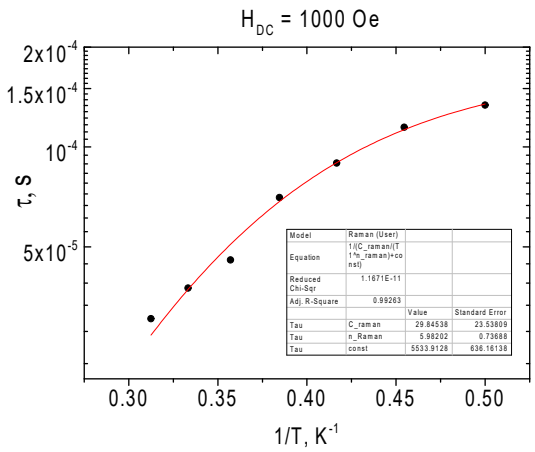

Raman+ QTM

$\tau^{-1} = C_{\text{Raman}} T^{\text{nRaman}} + \text{B}$

T = 2–3.2K

C_{Raman}= 30±24 $s^{-1}K^{-\text{nRaman}}$

n_{Raman}= 6.0±0.7

B = 5533±636 s^{-1}

R^2 = 0.99263

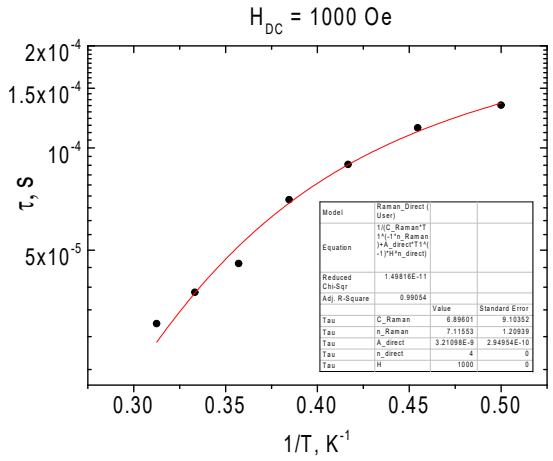

Raman+Direct

$\tau^{-1} = C_{\text{Raman}} T^{\text{nRaman}} + A_{direct} T H^4$

T = 2–3.2K

C_{Raman}= 6.8±9$s^{-1}K^{-\text{nRaman}}$

n_{Raman}= 7.1±1.2

A_{direct} = $3 \cdot 10^{-9} \pm 3 \cdot 10^{-10}$ $K^{-1}Oe^{-4}s^{-1}$

R^2 = 0.99054

Meaningless fit!!!

Table S10. CASSCF computed energy levels (the composition of the effective g′- tensor (assuming a pseudospin S = ½)and major (>10%) components of the wave function for each mJ state of the lowest atomic multiplet J=9/2 of Nd3+. KDs involved in magnetic relaxation are specified.

KD	E,K	g_x	g_y	g_z	Wavefunction decomposition, %
1	0.0	0.366	1.941	4.164	52|±9/2>26|±5/2>12|±1/2>
2	141.7	3.089	1.734	0.345	15|±9/2>29|±7/2>10|±5/2>27|±3/2>20|±1/2>
3	261.9	0.447	1.195	4.794	18|±9/2>24|±7/2>14|±5/2>10|±3/2>35|±1/2>
4	397.5	3.152	2.526	0.513	28|±7/2>41|±3/2>24|±1/2>
5	490.1	0.584	2.011	3.651	13|±9/2>15|±7/2>46|±5/2>16|±3/2>10|±1/2>

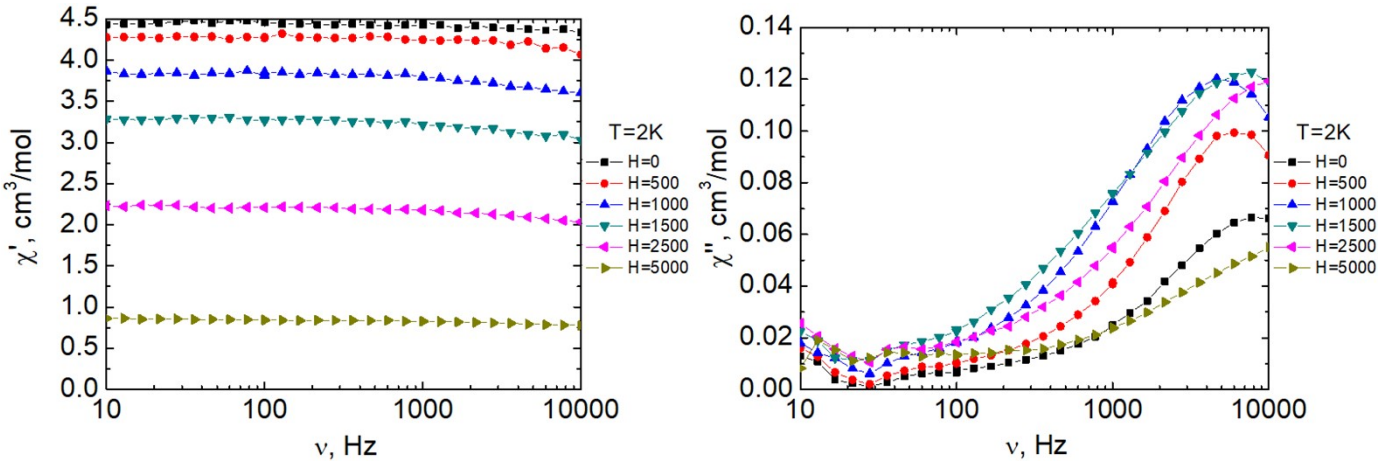

Fig. S12. Frequency dependencies of the in-phase (χ', left) and out-of-phase (χ'', right) components of the dynamic magnetic susceptibility of complex **Ho** measured at T=2K under various DC magnetic fields. Solid lines are visual guides.

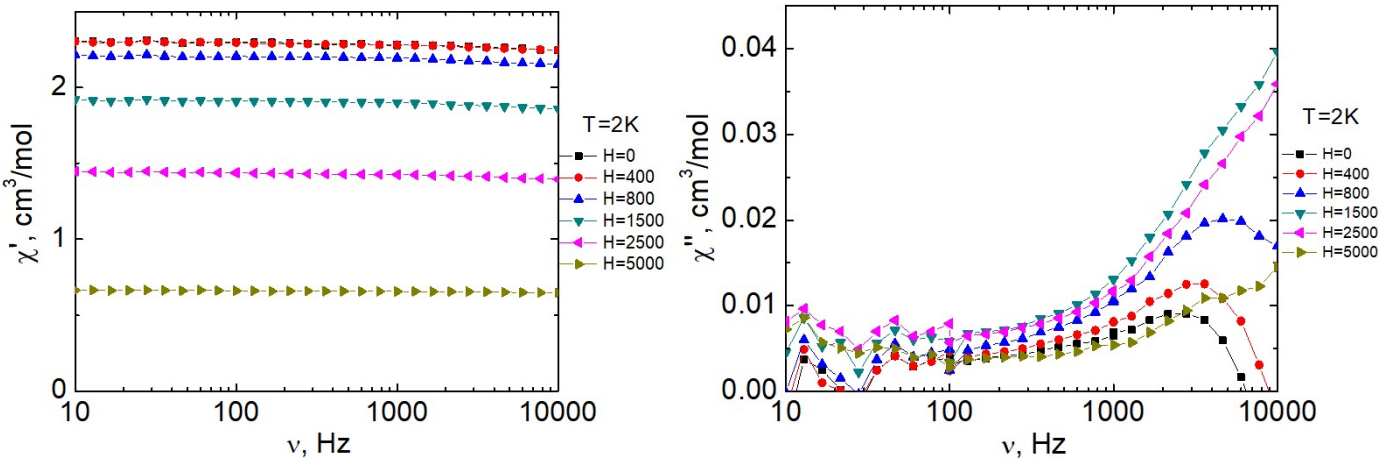

Fig. S13. Frequency dependencies of the in-phase (χ', left) and out-of-phase (χ'', right) components of the dynamic magnetic susceptibility of complex **Tm** measured at T=2K under various DC magnetic fields. Solid lines are visual guides.